

# Spectral study of decaparsec-scale radio jets



A. B. Pushkarev<sup>1,2</sup>

<sup>1</sup>Pulkovo Observatory; <sup>2</sup>Crimean Astrophysical Observatory



## Abstract

We report on an ongoing effort to image active galactic nuclei simultaneously observed at 2.3 and 8.6 GHz in the framework of a long-term geodetic VLBI program. The observations begun in 1994 with five-six sessions per year. All ten VLBA antennas together with up to ten additional (geodetic and EVN) radio telescopes participated in the observations. We present first-epoch results for 222 sources observed within one year (March 2002 – March 2003). We show total intensity images and scrutinize quality of our calibration. We discuss variable angular sizes, brightness temperature, spectral properties and optical depth of VLBI jets, particularly ones for the cores.

## Introduction

Long-term VLBI project RDV aimed at observations of compact extragalactic radio sources was started in 1994 under coordination of NASA and NRAO. The observations are carried out bi-monthly making up to five-six sessions per year with participation of all ten VLBA antennas and up to nine geodetic and EVN stations. Sample of observing objects consist of  $\sim 400$  sources from ICRF catalogue. In each experiment 80-90 AGN are observed and about 50 sources form a core of the sample scheduled in each session. The sample is dominated by quasars, with the weak-lined BL Lacs and radio-galaxies making up 16% and 6% of the sample, respectively. The project is focused on astrometry and geodesy problems, but the same data can also be used for astrophysical applications: mapping sources, modeling their structure, and doing all consecutive analysis. For these purposes we obtained the data from the NRAO archive. Since our first efforts were concentrated on initial data calibration (amplitudes and phases), first of all, we collected information about gain curves and system temperatures from the staff of the GEO/EVN radio telescopes.

A part of RDV experiments has been reduced by Alan Fey. We present the next part of monitoring data taken from seven consecutive sessions.

## Observations and Data Reduction

Seven experiments (RDV31, 32, 33, 34, 35, 36, 37) duration of 24h each were carried out on 2002 January 16-17, March 6-7, May 8-9, July 24-25, September 25-26, December 11-12, and 2003 March 12-13, respectively. The observations were made simultaneously at 2.3 and 8.6 GHz in right circular polarisation with 4 IFs, each 8 MHz wide. In addition to ten VLBA antennas 14 non-VLBA stations listed below were used in the sessions: Algopark (46m), Gilcreek (26m), HartRAO (26m), Kokee (20m), Matera (20m), Medicina (32m), Noto (32m), NRAO32 (20m), Ny Alesund (20m), Onsala (20m), TIGO (6m), Tsucuba (32m), Westford (18m), Wettzell (20m). Due to the large number of antennas participated in the experiments (usually 18-19) and located around the world, the whole array are divided on 7-8 subarrays. This allows for each station to work in a non-stop regime, tracking different targets in different subarrays. The north-south resolution provided by these observations is substantially improved in comparison with the VLBA only due to the use of the southern antennas in South Africa and Chile. The maximum baseline projection reached in the RDV experiments is about 12 000 km between Brewster and HartRAO, which is close to the limit for Earth-based VLBI observations. Each source, in average, had six scans of observations with total tracking time of approximately 50 minutes. There were no calibrators included in the schedule since all the sources were strong and compact. Usage 8-9 GEO/EVN radio telescopes dramatically increases the number of baselines (and visibilities as well) making the array roughly two times more sensitive and getting higher its angular resolution. The example of uv-coverages taken at 8.6 GHz for J1310+3220 (as a source having the number of visibilities close to the average value over the experiments) is shown in Figure 1.

The data were correlated using the VLBA correlator with integration time of 4 sec. The correlated data were calibrated and corrected for residual delays using the AIPS (NRAO) taking into account that the data are subarrayed. The initial amplitude calibration was done using system temperature measurements taken during the observations and the gain curves. Fring-fitting was done using solutions on 4 minute intervals and a point-source model and with cutoff of  $\text{SNR} \geq 5$  in all cases. All subsequent processing was carried out in DIFMAP (Shepherd 1997). The visibility data for each frequency band were self-calibrated, Fourier inverted, and CLEANed using an automatic script (Pearson 1994). A point-source model was used as a starting model for all objects. Convergence was usually obtained on average in 17 iterations (including phase-only and phase-and-amplitude self-calibration). The individual IFs were kept separate throughout the data reduction, and were averaged together only when making the final images.

Based on comparison of compact sources to near-simultaneous RATAN-600 measurements, we estimate that the accuracy of the absolute flux density scaling is  $\sim 10\%$ .

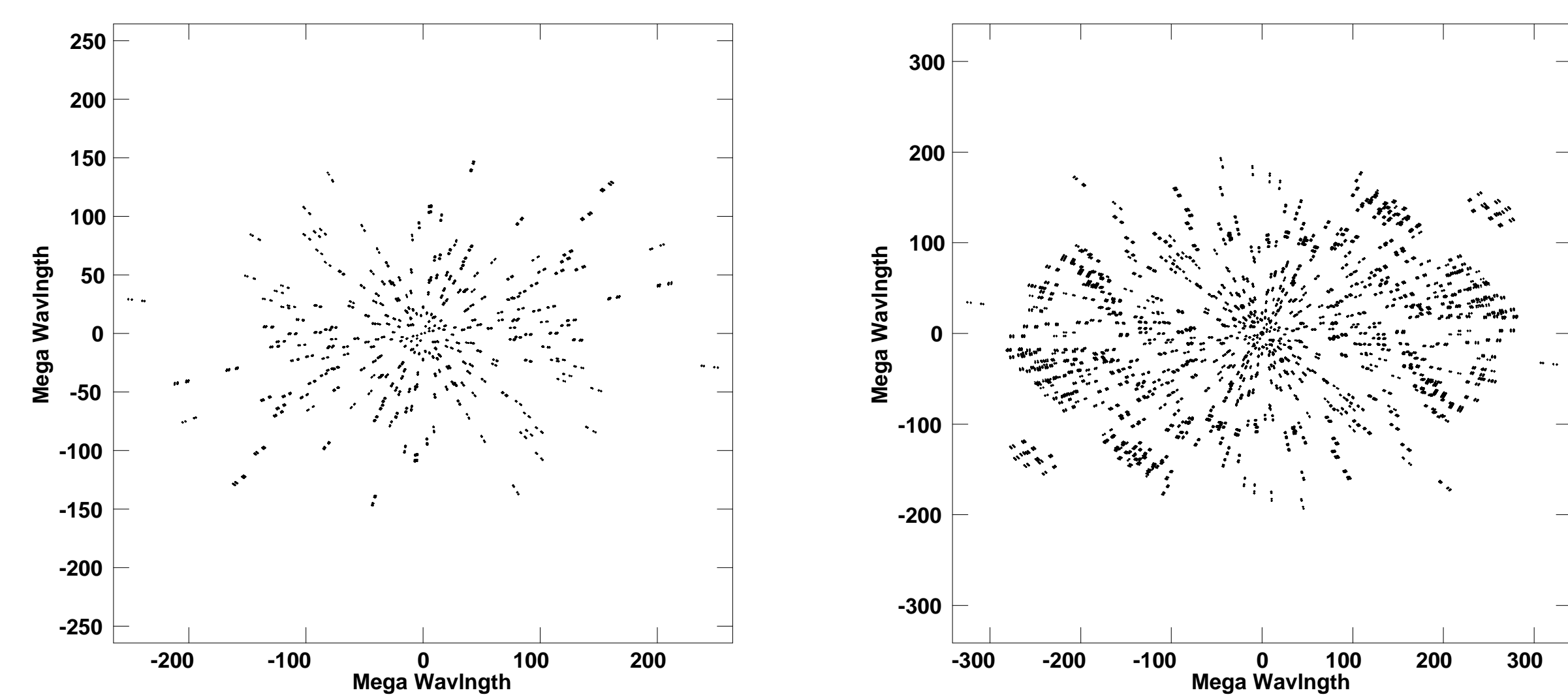


Figure 1. *uv*-coverages for J1310+32208 at 8.6 GHz produced only by VLBA antennas (left) and together with GEO/EVN stations (right).

## References

Shepherd, M. C., 1997, in ASP Conf. Series, 125, Astronomical Data Analysis Software and Systems VI, ed. G. Hunt & H. E. Payne (San Francisco: ASP), 77  
 Pearson, T. J., Shepherd, M. C., Taylor, G. B., & Myers, S. T., 1994, BAAS, 185, 0808  
 Kovalev, Y. Y., Kellermann, K. I., Lister, M. L., Homan, D. C., et al., 2005, AJ, 130, 2473

## Discussion

### Characteristics of the sample:

Here we present first-epoch results for 222 active galactic nuclei. All images taken at 2.3 and 8.6 GHz as well as visibility data and estimations of total and unresolved fluxes are available at <http://lacerta.gsfc.nasa.gov/vlbi/images>. The sample is dominated by blazars with a parsec-scale morphologies consisting of a bright and compact core component and a one-sided jet. Typical example of such structure is presented in Figure 2 by CLEAN images of BL Lac object J1800+7828. In rare cases (e.g., J0646+4451, J0449+1121, J1753+2848) no actual jet is evident, implying that the jet lies below the resolution or sensitivity level of observations.

Since we work with a relatively high number of sources, many of our results are statistical in nature. The maximum dynamic range of the taken images is  $\sim 4000:1$  at the S-band and  $\sim 6800:1$  at the X-band, while the average dynamic range is  $\sim 1200:1$  and  $\sim 1300:1$ , and average rms noise is  $\sim 0.68 \text{ mJy beam}^{-1}$  and  $\sim 0.62 \text{ mJy beam}^{-1}$ , respectively.

Simultaneous VLBI observations at two frequencies provide us with a possibility to analyze spectral properties of sources on parsec scales. Using the images at 2.3 and 8.6 GHz convolved with identical beam parameters and pixel size we can construct a spectral index distribution map ( $S \sim \nu^{\alpha}$ ) for all sources. Figure 3 (top) shows an example of such a map for the source J1800+7828. The region of the VLBI core has a flat spectrum (optically thick synchrotron emission), while moving down the jet the spectrum is getting steeper (optically thin synchrotron emission). This is easy to see on Figure 3 (bottom) where spectral index is plotted as a function of distance from the VLBI core along the central ridge line of the jet.

All the observed sources are relatively bright and compact. Figure 4 shows the distributions of total fluxes  $S_{\text{VLBA+}}$  (collected from the maps) with approximately the same median values of 0.8 Jy at S- and X-band. The sources are core-dominated (Figure 5, top) and compact (Figure 5, bottom) with the median index of compactness of 0.51 at S-band and 0.53 at X-band, calculated as  $S_{\text{unres}}/S_{\text{VLBA+}}$ , where  $S_{\text{unres}}$  is the correlated flux densities averaged only over projected baselines longer than 70 M $\lambda$  at S-band and 270 M $\lambda$  at X-band, which correspond to the  $h$  range [0.8, 1.0] of the maximum projected spacings of the arrays.

The statistics of integral spectral index is presented on Figure 6 (left) showing that the majority of sources have flat spectra between 2.3 and 8.6 GHz with a median value of spectral index of  $-0.01$ . There is a weak but detectable tendency for sources with steeper spectra to be less compact. It seems natural since steep spectrum sources have significant part of emission in their jets.

The distributions of estimated values and lower limits of VLBI core brightness temperature (calculated in the observer frame and shown in Figure 7) are very broad, spanning five orders of magnitude, but with a prominent peak at approximately  $10^{11} \text{ K}$  at both frequencies. The lower limits on  $T_b$  were calculated assuming a minimal resolvable component size following Kovalev et al. (2005).

**We plan** to continue our efforts of imaging sources at other available epochs, to extract all valuable information from structure modeling: a) to analyze brightness temperatures for jet components and its evolution, b) to estimate optical depth of core and jet component emission as well as trace the spectral index steepening with a distance from the core, c) to investigate the core-shift effect, d) to measure and analyze the jet kinematics, compare with results from other frequencies.

The work is done in collaboration with Yuri Y. Kovalev (ASC LPI, NRAO).

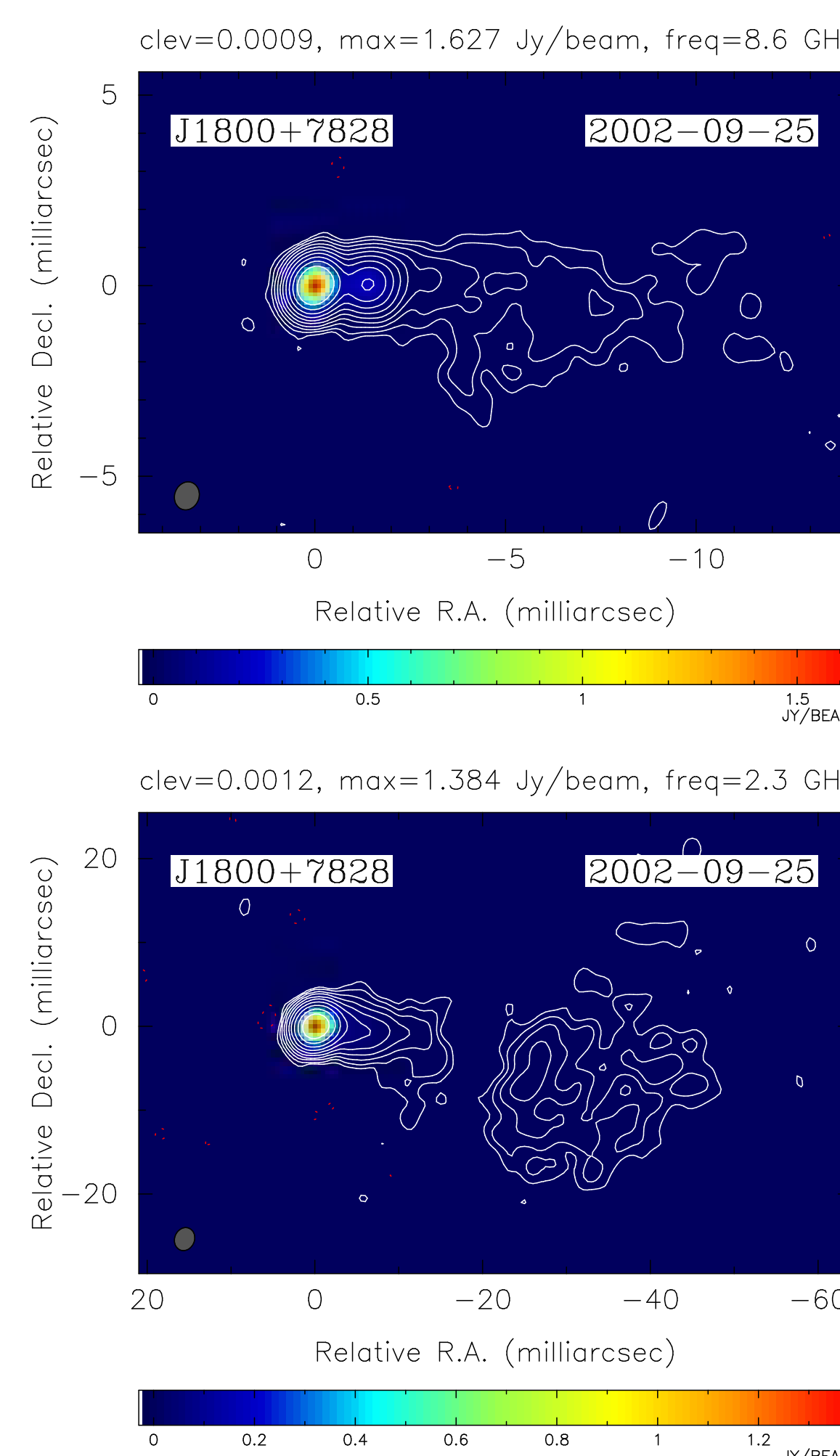


Figure 2. VLBI CLEAN images of J1800+7828 at X-band (top) and S-band (bottom) with contours increasing in steps of two.

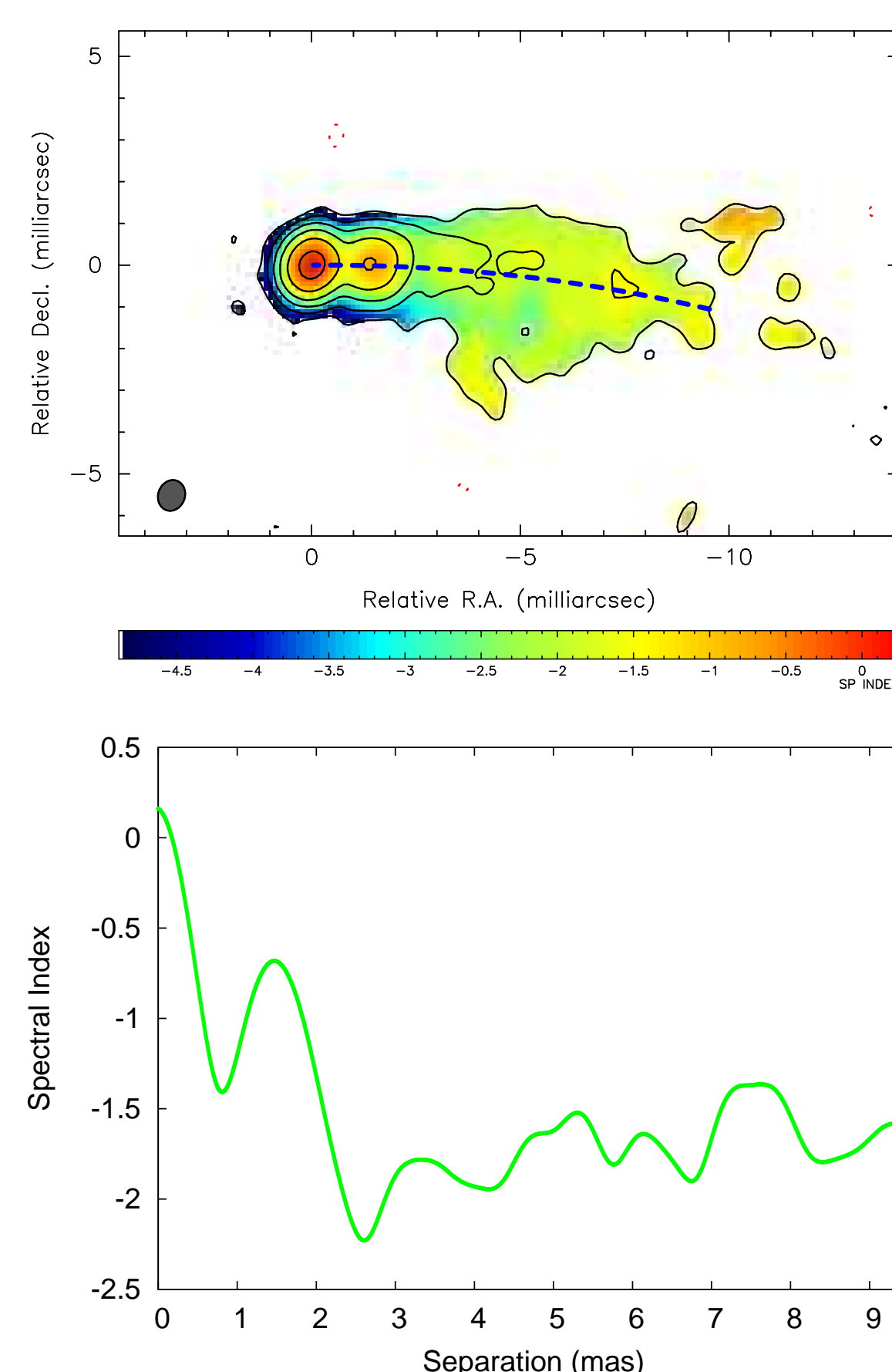


Figure 3. Spectral index distribution map over contours at 8.6 GHz (top). Dashed blue line indicates a central spine of the jet. Spectral index as a function of distance from the VLBI core along the jet ridge line (bottom).

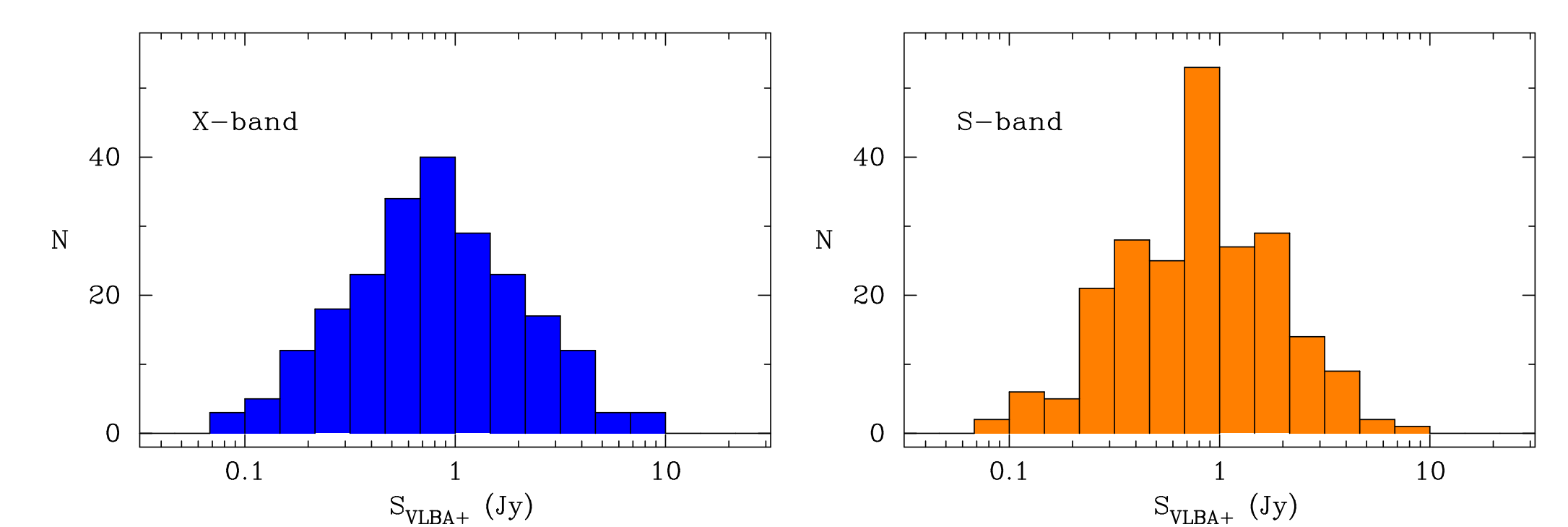


Figure 4. Distributions of total flux density of the 222 observed sources.

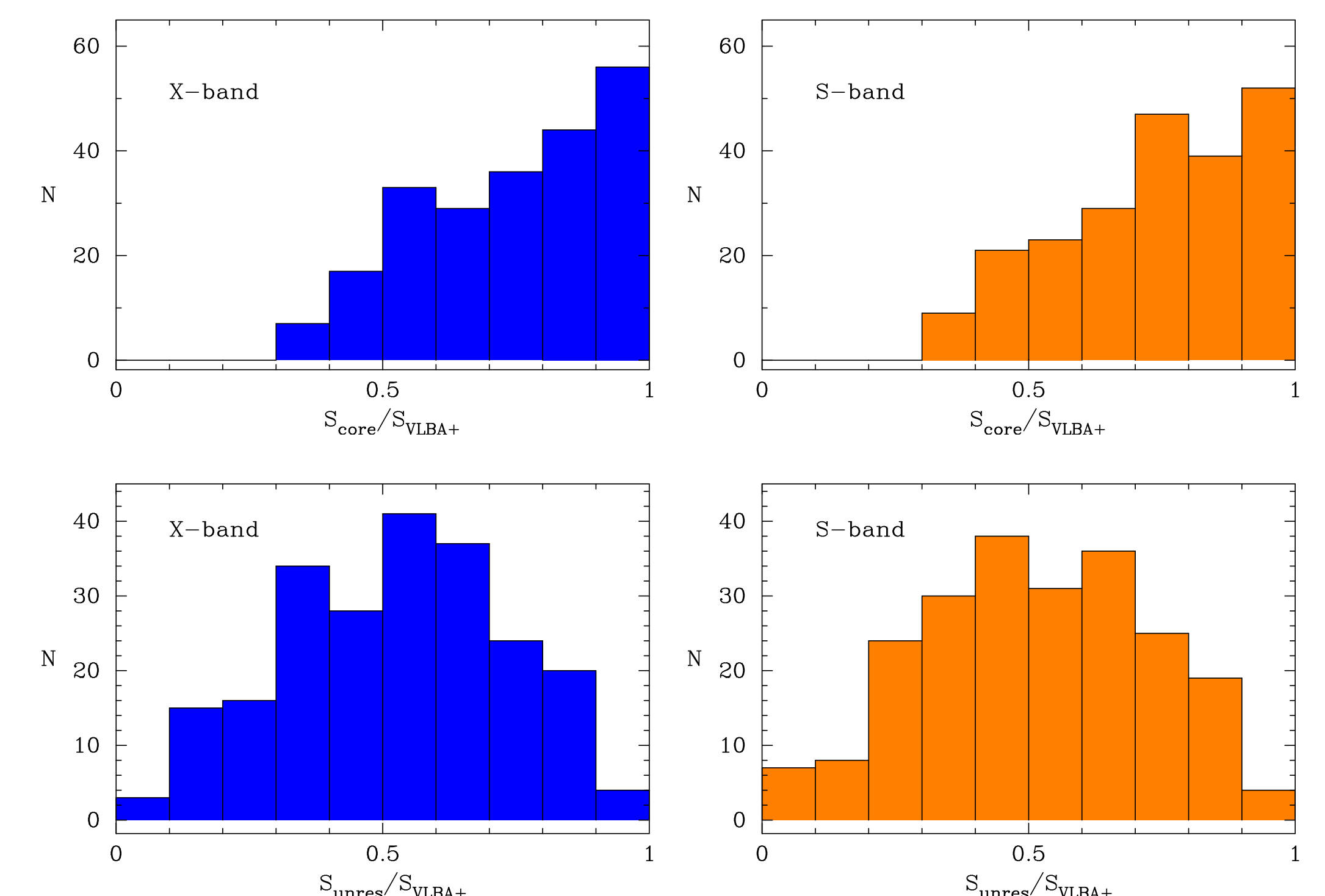


Figure 5. Distributions of VLBI core dominance  $S_{\text{core}}/S_{\text{VLBA+}}$  (top) and compactness indices  $S_{\text{unres}}/S_{\text{VLBA+}}$  (bottom).

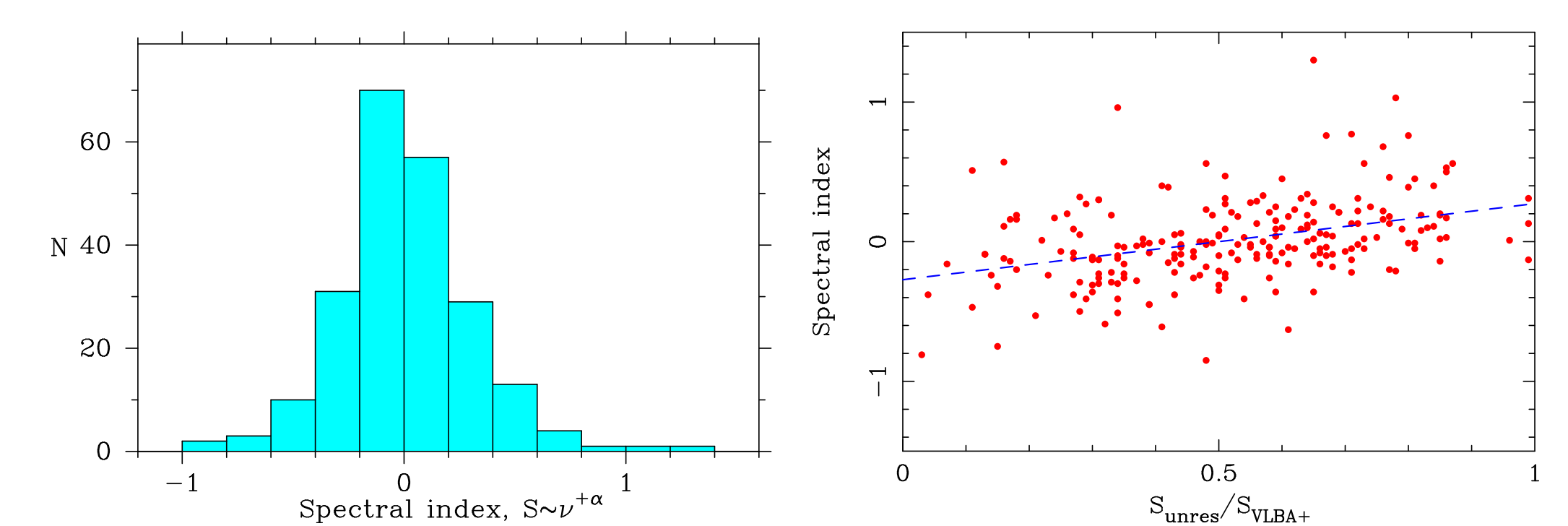


Figure 6. Distribution of integral spectral index (left) and spectral index versus compactness dependence (right).

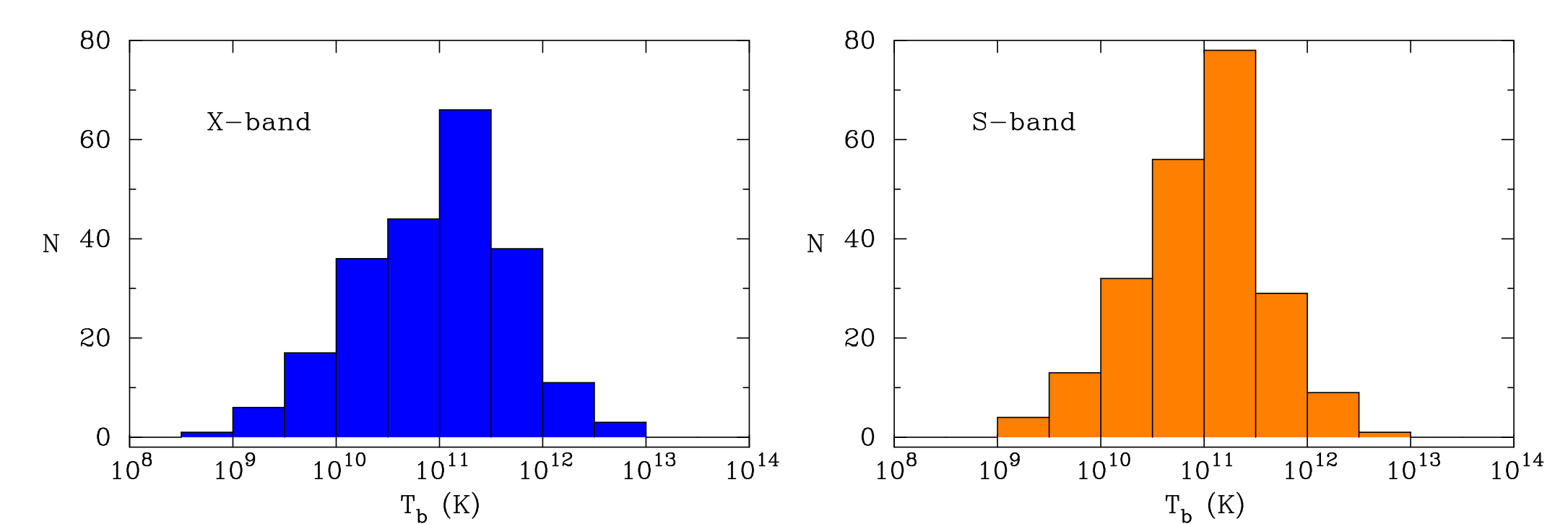


Figure 7. Distributions of the VLBI brightness temperature (including lower limits) in the observer frame at 8.6 GHz (left) and 2.3 GHz (right).